Scripta Materialia 233 (2023) 115515

Contents lists available at ScienceDirect

Scripta Materialia

journal homepage: www.journals.elsevier.com/scripta-materialia

Effect of Si on the hydrogen-based direct reduction of Fe_2O_3 studied by XPS of sputter-deposited thin-film model systems

Lena Patterer [a,*], Eva B. Mayer [a], Stanislav Mráz [a], Peter J. Pöllmann [a], Marcus Hans [a], Daniel Primetzhofer [b], Isnaldi R. Souza Filho [c], Hauke J. Springer [c,d], Jochen M. Schneider [a]

[a] Materials Chemistry, RWTH Aachen University, Kopernikusstr. 10, 52074 Aachen, Germany
[b] Department of Physics and Astronomy, Uppsala University, Lägerhyddsvägen 1, 75120 Uppsala, Sweden
[c] Max-Planck-Institut für Eisenforschung, Max-Planck-Str. 1, 40237 Düsseldorf, Germany
[d] Institute of Metal Forming, RWTH Aachen University, Intzestr. 10, 52072 Aachen, Germany

ARTICLE INFO

Keywords:
Hydrogen
X-ray photoelectron spectroscopy
Direct reduction of iron oxide
Silicon
Thin films

ABSTRACT

Understanding the effect of gangue elements is of critical importance to optimize the efficiency of hydrogen-based direct reduction (HyDR) of iron ore, as one of the key steps towards climate-neutral steel production. Here, we demonstrate on the example of Si-doped Fe_2O_3, how thin films can be effectively utilized as a model system to facilitate systematic investigation of the solid-state reduction behavior. *In-vacuo* X-ray photoelectron spectroscopy (XPS) is used to probe the reduction kinetics by analyzing the chemical state of iron oxide thin films before and after annealing at 700 °C in an Ar+5%H_2 atmosphere. It is demonstrated that even low Si concentrations of 3.7 at.% inhibit the HyDR of Fe_2O_3 by the formation of a SiO_x-enriched reduction barrier in the surface-near region.

The iron- and steelmaking industry is currently responsible for ~ 7% of global CO_2 emissions [1,2], motivating the substitution of carbon-carrier substances with hydrogen as a reducing agent for iron ores in order to produce H_2O instead of CO_2 as the direct by-product [3]. During hydrogen-based direct reduction (HyDR), iron ore pellets or fines are reduced in the solid state by H_2 gas at elevated temperatures [3]. Previous studies showed that a high reduction temperature and H_2 pressure, as well as an increased porosity and hematite (Fe_2O_3) concentration, rather than magnetite (Fe_3O_4), enhance the overall reduction kinetics of iron ores with H_2 [3]. Besides these factors, the impurities in iron ores have to be considered as well [3–5]. However, the effect of gangue-related oxides, such as SiO_2, CaO, or MnO_2, - always present in ores processed on the industrial scale - on the reduction process is less well understood.

For the already well-researched CO-based reduction at 800–1100 °C, as used e.g. in blast furnaces, it was reported that SiO_2-doping has a positive effect on the initial reduction stage of Fe_2O_3 compacts into Fe_3O_4 due to the increased porosity, but at advanced reduction stages, the competing formation of the iron silicate fayalite (Fe_2SiO_4 or $2FeO{\cdot}SiO_2$) significantly decreases the reduction rate with increasing SiO_2 content [4]. At 1000 °C, it was observed that SiO_2-doped FeO compacts are more readily reduced by H_2 compared to CO, but the reduction rate for both gases is always lower compared to the undoped FeO compacts [5]. In such cases, the porosity in SiO_2-doped FeO compacts decreases upon reduction treatment due to Fe_2SiO_4 formation, which slows down the reduction progress [5,6]. Additionally, it was shown, that the solid-state reduction of Fe_2SiO_4 by molecular hydrogen is thermodynamically unfavorable and kinetically sluggish [7,8].

In a theoretical study, it was demonstrated that the adsorption of SiO_2 onto the FeO(111) surface exhibits significantly larger absolute adsorption energy (5.72 eV) [9] compared to the reducing gases H_2 (0.65 eV [10]) and CO (1.41 eV [10]), indicating that SiO_2 adsorption is more favorable [9]. Also, once the O adsorption site is occupied by Si, it is more difficult to remove oxygen from FeO by reactions with H_2 or CO [9].

In the context of improving the oxidation resistance of steel, the effect of Si alloying was observed to cause the formation of a Fe_2SiO_4 sublayer between steel and its scale (iron oxide layers) upon the

Abbreviations: HyDR, hydrogen-based direct reduction; XPS, X-ray photoelectron spectroscopy; HPPMS, high power pulsed magnetron sputtering; ToF-ERDA, Time-of-flight elastic recoil detection analysis; RBS, Rutherford backscattering spectrometry; XRD, X-ray diffraction.

* Corresponding author.
E-mail address: patterer@mch.rwth-aachen.de (L. Patterer).

https://doi.org/10.1016/j.scriptamat.2023.115515
Received 25 February 2023; Received in revised form 19 April 2023; Accepted 22 April 2023

oxidation at 900–1200 °C [11]. Below 1177 °C, this sublayer functions as a diffusion barrier for Fe^{2+} ions and slows down the oxidation, whereas at higher temperatures Fe_2SiO_4 melts and the liquid at the steel-scale interface accelerates the oxidation [11,12].

In a recent study, a combined technological approach using solid-state HyDR at 700 °C for a partial reduction of iron ore, as well as subsequent application of a reducing hydrogen-containing plasma for melting and complete reduction to Fe was proposed, due to its efficient hydrogen and energy consumption [13]. As evident from the discussion above, most previous reduction studies focus on the influence of SiO_2 on iron oxide solid-state reduction at high temperatures (> 900 °C) [4–6,9,14] and are also defined by the morphology of the produced powder compacts. In contrast, the underlying chemical mechanisms that lead to the competing formation of iron silicates and their impact on the reduction remain unclear, especially for lower reduction temperatures. To shed light on that, we present here a novel research strategy to study the influence of Si on the HyDR of iron oxide by synthesizing dense undoped and Si-doped Fe_2O_3 thin films using magnetron sputtering. This allows for the investigation of iron oxides with a controlled chemical build-up and without the influence of otherwise difficult-to-control meso- and microstructural porosity. Subsequently, these thin films are annealed at 700 °C in an Ar+5%H_2 atmosphere to study the reduction kinetics by *in-vacuo* X-ray photoelectron spectroscopy (XPS). This study aims for a simplified model system to exclusively investigate the chemical effect of gangue elements on the hydrogen-based reduction behavior of Fe_2O_3. However, also other factors, such as porosity – affecting the surface area available for reduction – are expected to influence the reduction behavior and should, therefore, be systematically investigated to obtain a comprehensive picture of all mechanisms affecting the hydrogen-based reduction on the industrial scale.

In order to produce dense thin films, high power pulsed magnetron sputtering (HPPMS) is a commonly used deposition technique, as a high ionization degree of sputtered species is generated during the process, leading to a densification of the thin film by bombardment-induced adatom migration [15]. Hence, Fe_2O_3 thin films were grown by reactive HPPMS onto 1 × 1 cm^2 α-Al_2O_3(0001) substrates. A 0.9 mm-thick Fe disk (99.99% purity, Kurt J. Lesker Company GmbH) and a 500 μm-thick Si wafer (Siegert Wafer GmbH) utilized as targets (both having a diameter of 50 mm) were mounted with an angle of ~ 45° between target and substrate normal, while the target-to-substrate distance was ~ 10 cm. The base pressure before the deposition was always < 8 × 10^{-5} Pa and the total working pressure was 0.59 Pa with an Ar/O_2 ratio of ~ 9/1 (both 99.999% purity). During deposition without intentional substrate heating, the electrically floating substrate holder was rotated at a speed of 20 rpm. The Fe target was operated with a Melec SIPP2000USB-10-500-S pulser and a 10 kW ADL GP 15 power supply using a time-averaged power of 100 W, a pulse-on time of 50 μs, and a duty cycle of 2%, resulting in a peak power density of 0.7 kW cm^{-2}. For the Fe_2O_3 + Si deposition, the Si target was operated by using a PowerCube plain 13–400 generator with a MatchingCube i-600 matchbox (barthel HF-Technik GmbH) and applying an RF power of 20 W. No interference between the HPPMS and RF plasmas due to different frequencies was identified during the deposition and the tracked HPPMS peak current stayed constant between both Fe_2O_3 and Fe_2O_3+Si depositions. All depositions were carried out for 60 min resulting in a film thickness of ~ 200 nm.

Time-of-flight elastic recoil detection analysis (ToF-ERDA) of the as-deposited samples and a sapphire reference sample was performed at the tandem accelerator laboratory of Uppsala University [16] by using a $^{127}I^{8+}$ ion beam with a primary energy of 36 MeV. In order to enhance the measurement accuracy in a self-consistent approach, the ToF-ERDA data was combined with Rutherford backscattering spectrometry (RBS) [17] using 2 MeV $^4He^+$ ions. More details can be found elsewhere [18].

XPS survey scans, as well as high-resolution Fe 2p, Si 2 s, and valence-band spectra, were acquired before and after the reduction treatment of the samples in an AXIS Supra instrument (Kratos Analytical Ltd.) with a base pressure < 1.3 × 10^{-6} Pa using monochromatic Al Kα radiation. Charge neutralization was applied during acquisition and the binding energy (BE) scale was calibrated by fitting a step-down function to the pronounced Fermi edge of Fe_2O_3 and setting it to 0 eV using the CasaXPS software package (Casa Software Ltd.). The spectrometer was calibrated by using a sputter-cleaned Ag foil (BE of Ag $3d_{5/2}$ = 368.2 eV). The elemental quantification of the survey scan was performed by subtracting a Shirley background [19] and applying the manufacturer's sensitivity factors [20].

During the reduction treatment in the pre-chamber of the XPS instrument (p_{base} < 1.7 × 10^{-5} Pa), the samples were heated up to 700 °C using a heating rate of 20 K/min in an Ar+5%H_2 atmosphere (Ar-5 vol. % H_2 gas mixture) with a total pressure of ~ 1 Pa. The samples were isothermally annealed at 700 °C for 1 h and subsequently cooled at a rate of 20 K/min until the sample temperature reached < 50 °C. Afterwards, the Ar+5%H_2 gas flow was stopped, and the sample was transferred *in-vacuo* back into the XPS analysis chamber.

The crystallographic structures of the thin films before and after reduction treatment were examined by X-ray diffraction (XRD) in a Siemens D5000 system with Bragg-Brentano geometry applying Cu Kα radiation with an acceleration voltage and current of 40 kV and 40 mA, respectively.

The chemical composition of the as-deposited thin films determined by ToF-ERDA is shown in Table 1. The undoped Fe_2O_3 thin film with an atomic O/Fe ratio of 1.52 ± 0.02 is in very good agreement with the expected stoichiometry of 1.50 for hematite (α-Fe_2O_3). When Si is included in the deposition process, the O concentration is slightly higher compared to the undoped thin film (+1.1 ± 0.4 at.%), whereas the iron concentration is decreased. The ToF-ERDA results are consistent with RBS data, and depth profiles were found very homogenous.

When analyzing the XPS Fe 2p signal (Fig. 1), information about the chemical state of iron atoms is obtained. The as-deposited undoped Fe_2O_3 thin film exhibits a peak at the Fe(III) oxidation state at binding energy (BE) ~ 709.8 eV [21] (red curve, Fig. 1). The characteristic Fe (III) satellite signal was reported to be shifted by +7.8 eV relative to the main Fe(III) signal [22], leading here to a signal at BE ~ 717.6 eV (red curve). After annealing the undoped Fe_2O_3 thin film at 700 °C in an Ar+5%H_2 atmosphere (yellow curve), two shoulders at lower BE appear, indicating the reduction of Fe(III) to Fe(II) (BE ~ 708.4 eV) and metallic Fe^0 (BE ~ 706.5 eV). Naturally, also the Fe(III)-satellite signal is decreased compared to the as-deposited state, and the Fe(II)-satellite signal at BE ~ 715.4 eV appears. The observed +7 eV shift of the Fe (II)-satellite signal relative to the main Fe(II) signal is consistent with literature [22]. When the Fe_2O_3 thin film is doped with 3.7 at.% Si, no significant differences in the Fe 2p signal are obtained for the as-deposited state compared to the undoped thin film (violet vs. red curve). However, when the Si-doped thin film is annealed at 700 °C in an Ar+5%H_2 atmosphere, the reduction appears to be less efficient compared to the undoped sample (blue vs. yellow curve). In Fe_2SiO_4, Fe has an oxidation state of +II ($2FeO{\cdot}SiO_2$) and a BE shift of -0.5 eV relative to the Fe(II) signal of $Fe_{0.94}O$ (wuestite) was reported in literature [22]. Based on this information, it is reasonable to assume that the here observed shoulder at BE ~ 707.7 eV (blue curve in Fig. 1) contains Fe_2SiO_4 contributions.

By analyzing the XPS survey spectra of the thin films before and after the reduction treatment, the change in the O-to-Fe ratio at the surface is determined (Fig. 2). Surface oxidation and the XPS probing depth of

Table 1
Chemical composition of as-deposited thin films (ToF-ERDA) and statistical uncertainty.

	Fe (at.%)	O (at.%)	Si (at.%)	O/(Fe+Si)
undoped Fe_2O_3	39.7 ± 0.3	60.3 ± 0.3	–	1.52 ± 0.02
Si-doped Fe_2O_3	34.9 ± 0.4	61.4 ± 0.4	3.7 ± 0.2	1.59 ± 0.03

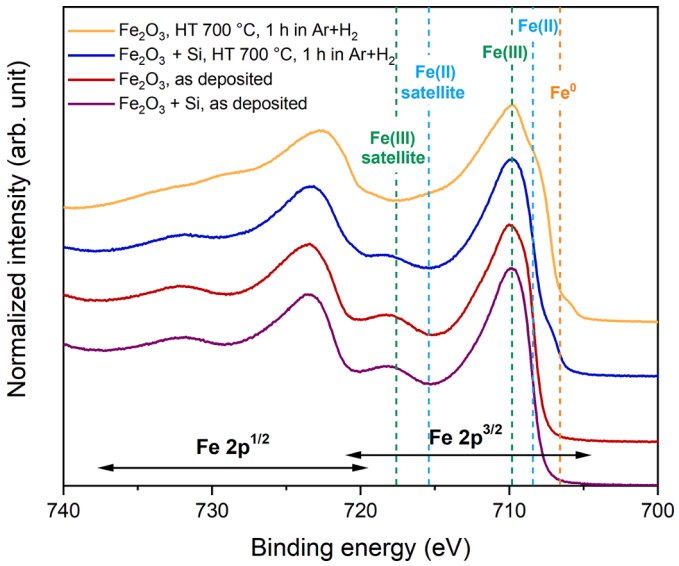

Fig. 1. XPS Fe 2p signals of undoped and Si-doped Fe_2O_3 thin films before and after annealing at 700 °C in Ar+5%H_2 atmosphere (1 h). The BEs of Fe^0 (orange), Fe(II) (light blue), Fe(III) (green) oxidation states and their corresponding satellite signals (light blue, green) are marked by the colored dashed lines [21,22].

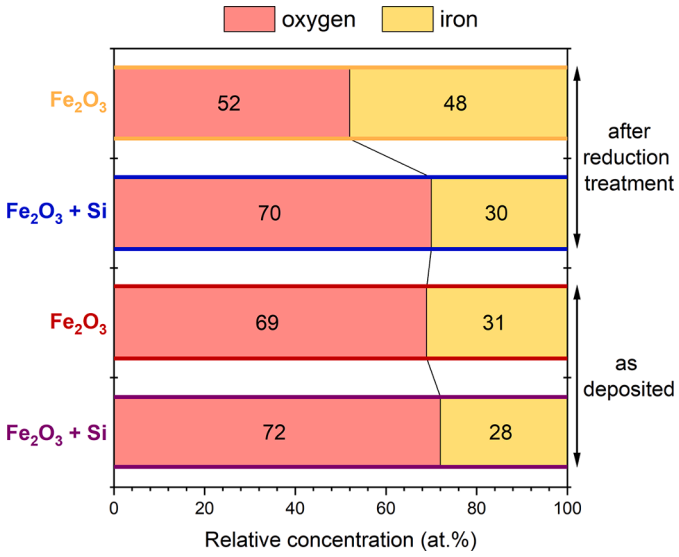

Fig. 2. The surface oxygen-to-iron ratio of undoped and Si-doped Fe_2O_3 thin films before and after annealing at 700 °C in an Ar+5%H_2 atmosphere (1 h) measured by in-vacuo XPS.

only 5–10 nm [23] result in a higher O concentration compared to the composition measured by ToF-ERDA (Table 1). From Fig. 2, a similar ratio for the as-deposited undoped and Si-doped Fe_2O_3 thin films is evident (violet- and red-framed bar). After the reduction treatment, the undoped sample (yellow-framed bar) exhibits a significant increase in the Fe concentration (Fig. 2) indicating a reduction reaction with H_2, whereas the ratio for the Si-doped Fe_2O_3 thin film (blue-framed bar) is almost unchanged. This inhibiting effect of Si on the reduction agrees very well with the insights gained from the analysis of the Fe 2p signal (Fig. 1), as Fe(II) and Fe^0 signals were detected for the undoped thin film, while only a small signal of Fe(II) - very likely with Fe_2SiO_4 contributions - appears for the Si-doped Fe_2O_3 thin film, implying a less efficient reduction for the Si-doped samples.

When comparing the Si 2 s signal for the Si-doped Fe_2O_3 thin film before and after the reduction treatment (Si 2p signal is disturbed by Fe 3 s contributions), a BE shift of +1 eV is evident (Fig. 3). Additionally, the analysis of the respective survey scans indicates an increase in the atomic Si-to-Fe ratio (Fig. 3). The peak shift towards higher BE demonstrates that Si exhibits a higher oxidation state after the reduction treatment [24], while the increase of the Si-to-Fe ratio reveals a Si enrichment at the surface. Hence, the XPS analysis of the Si-doped Fe_2O_3 thin film (Fig. 3) suggests the formation of a SiO_x-enriched surface region upon annealing at 700 °C in an Ar+5%H_2 atmosphere, which inhibits the hydrogen-based reduction of the subjacent thin film. This observation is in good agreement with the reported formation of Fe_2SiO_4 for SiO_2-doped iron oxide compacts, which were subjected to reduction experiments at higher temperatures and with different reducing agents [4,5,9].

Additionally, XRD measurements of the thin films before and after the reduction treatment were performed (Fig. 4). In contrast to XPS, XRD exhibits a larger probing depth (typically in the μm range). The as-deposited Fe_2O_3 thin film shows a single peak at $2\theta = 38.8°$ (red curve, Fig. 4) indicating a strongly textured phase formation, which is typical for films grown by magnetron sputtering [25]. The peak is slightly shifted relative to the reported value of 39.3° for the (006) plane of α-Fe_2O_3 (hematite) [26]. This shift may be explained by residual compressive stress in the thin film due to the expected lattice mismatch with the α-Al_2O_3(0001) substrate [27]. Moreover, the stress may also result from the dense microstructure caused by the high density of ions during HPPMS, which gain - due to the floating potential at the substrate – some additional kinetic energy by experiencing acceleration towards the substrate [28]. Combining the results from XRD with the previous insights obtained from the chemical composition (O/Fe ~ 1.52 ± 0.02) and the chemical state (Fe(III)), it is reasonable to assume that the XRD peak visible for the as-deposited Fe_2O_3 thin film belongs to the phase of α-Fe_2O_3 (hematite). The diffractogram of the as-deposited Si-doped Fe_2O_3 (violet curve, Fig. 4) shows a peak shifted to even lower angles compared to the undoped sample, which might be due to additional compressive stress and/or lattice distortion (larger lattice spacing *d*) by the introduction of Si atoms into the interstitial sites of the lattice. While the Si-doped Fe_2O_3 thin film may or may not exhibit a different phase compared to the undoped variant, after annealing, the single peak of the Si-doped Fe_2O_3 (blue curve, Fig. 4) shifts towards the peak position of the undoped Fe_2O_3 thin film (red), implying that Si is diffusing out of the

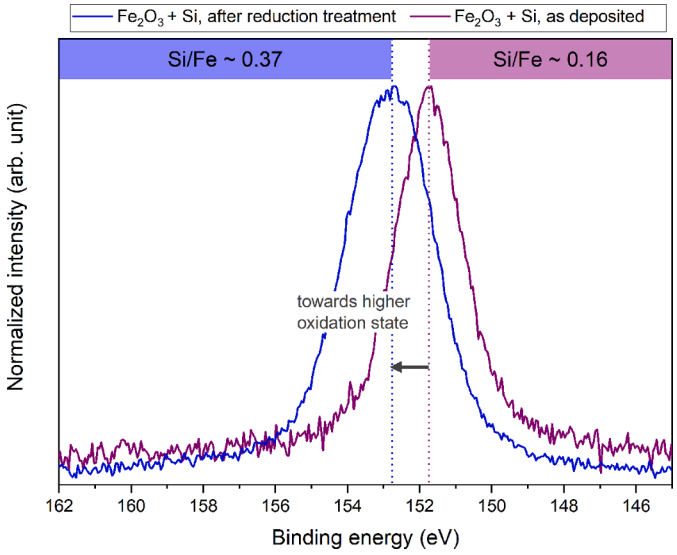

Fig. 3. Normalized XPS Si 2 s signal of Si-doped Fe_2O_3 before (violet) and after (blue) annealing at 700 °C in an Ar+5%H_2 atmosphere (for 1 h). Additionally, the atomic Si-to-Fe ratio determined from the survey scans is shown for both samples.

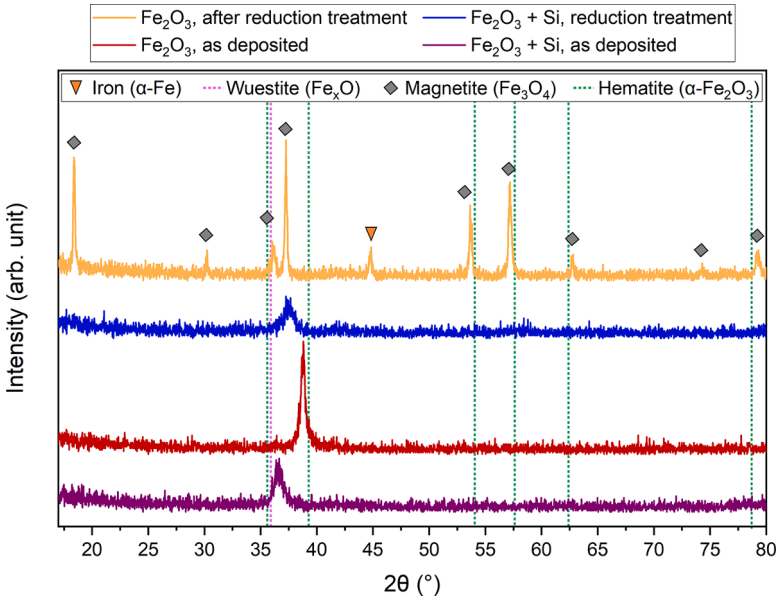

Fig. 4. Diffractograms of the undoped and Si-doped Fe_2O_3 thin films before and after annealing at 700 °C in an Ar+5%H_2 atmosphere (1 h) measured by XRD. The literature 2θ values of iron (α-Fe) [29], wuestite (Fe_xO) [30], magnetite (Fe_3O_4) [31], and hematite (α-Fe_2O_3) [26] for the relevant peak positions are indicated by colored symbols and dashed lines.

Fe_2O_3 lattice towards the surface as already indicated by the XPS-measured SiO_x surface enrichment. This peak shift upon the reduction treatment towards the peak position of the untreated, undoped Fe_2O_3 is an indicator that the Si-doped Fe_2O_3 exhibits the same phase with an expanded lattice caused by incorporated Si. Future *in-situ* diffraction experiments during annealing are expected to resolve this issue.

When considering the reduced undoped Fe_2O_3 thin film (yellow curve, Fig. 4), a wide range of new peaks appear compared to the as-deposited sample, suggesting the presence of Fe_3O_4 (magnetite, grey marker [31]) and α-Fe (iron, orange marker [29]), and also, a small fraction of Fe_xO (wuestite) is indicated by a signal at $2\theta = 36.1°$ (pink dashed line [30]).

The XRD data confirms that the undoped Fe_2O_3 thin film is significantly reduced by the H_2 treatment at 700 °C – also beyond the ~ 10 nm-probing depth of XPS - as signals of phases with lower oxidation states (Fe_3O_4, Fe_xO, α-Fe) are detected. Contrarily, the annealed Si-doped Fe_2O_3 sample only exhibits a peak shift compared to the as-deposited sample, and the formation of phases indicating reduction cannot be resolved, demonstrating further the inhibiting effect of Si on the HyDR of Fe_2O_3.

This *in-vacuo* XPS study of dense undoped and Si-doped Fe_2O_3 thin films deposited by HPPMS demonstrates an efficient way to examine exclusively the chemical effect - independent of microstructural defects such as porosity and cracks - of typical gangue elements on the HyDR of iron oxide in a controlled and systematic manner. The investigation reveals that the doping of 3.7 at.% Si significantly inhibits the HyDR of Fe_2O_3 at 700 °C by forming a SiO_x-enriched layer in the surface-near region. It is shown that this chemical transformation has the potential to locally cease the progress of reduction by blocking free surfaces of iron oxides, and thereby, impeding the direct contact with reducing agents. This research strategy may also be readily adapted to other typical gangue elements of iron ores to examine their influence on the HyDR, thus helping to properly adjust the chemical composition of feedstocks and paving the way to more sustainable and climate-neutral iron ore reduction processes.

CRediT authorship contribution statement

Lena Patterer: Conceptualization, Methodology, Formal analysis, Investigation, Writing – original draft, Visualization. **Eva B. Mayer:** Methodology, Formal analysis, Investigation, Writing – review & editing. **Stanislav Mráz:** Methodology, Investigation, Writing – review & editing. **Peter J. Pöllmann:** Methodology, Formal analysis, Investigation, Writing – review & editing. **Marcus Hans:** Formal analysis, Investigation, Writing – review & editing. **Daniel Primetzhofer:** Formal analysis, Investigation, Writing – review & editing. **Isnaldi R. Souza Filho:** Conceptualization, Methodology, Writing – review & editing. **Hauke J. Springer:** Conceptualization, Methodology, Writing – review & editing. **Jochen M. Schneider:** Conceptualization, Methodology, Writing – original draft, Supervision, Project administration, Funding acquisition.

Declaration of Competing Interest

The authors declare that they have no known competing financial interests or personal relationships that could have appeared to influence the work reported in this paper.

Acknowledgments

Transnational access to the ion-beam analysis facility at Uppsala University has been supported by the RADIATE project under the Grant Agreement 824096 from the EU Research and Innovation program Horizon 2020. Accelerator operation at Uppsala University has been supported by the Swedish research council VR-RFI (#2019-00191).

References

[1] D. Raabe, C.C. Tasan, E.A. Olivetti, Strategies for improving the sustainability of structural metals, Nature 575 (2019) 64–74.
[2] Y. Ma, I.R. Souza Filho, Y. Bai, J. Schenk, F. Patisson, A. Beck, J.A. van Bokhoven, M.G. Willinger, K. Li, D. Xie, D. Ponge, S. Zaefferer, B. Gault, J.R. Mianroodi, D. Raabe, Hierarchical nature of hydrogen-based direct reduction of iron oxides, Scr. Mater. 213 (2022), 114571.
[3] D. Spreitzer, J. Schenk, Reduction of iron oxides with hydrogen—a review, Steel Res. Int. 90 (2019), 1900108.

[4] A.-H.A. El-Geassy, M.I. Nasr, A.A. Omar, E.-S.A. Mousa, Influence of SiO_2 and/or MnO_2 on the reduction behaviour and structure changes of Fe_2O_3 compacts with CO gas, ISIJ Int. 48 (2008) 1359–1367.
[5] W.-.H. Kim, Y.-.S. Lee, I.-.K. Suh, D.-.J. Min, Influence of CaO and SiO2 on the reducibility of wuestite using H2 and CO Gas, ISIJ Int. 52 (2012) 1463–1471.
[6] M. Bahgat, K.S. Abdel Halim, M.I. Nasr, A.A. El-Geassy, Morphological changes accompanying gaseous reduction of SiO 2 doped wüstite compacts, Ironmak. Steelmak. 35 (2008) 205–212.
[7] G.C. Ulmer, W.C. Elliott, T. Buntin, E.S. Erickson, J.J. Friel, Role of selected cations and gas speciation on the reduction of fayalite at 1300 °C, J. Am. Ceram. Soc. 75 (1992) 1476–1483.
[8] C.C. Massieon, A.H. Cutler, F. Shadman, Hydrogen reduction of iron-bearing silicates, Ind. Eng. Chem. Res. 32 (1993) 1239–1244.
[9] Z. Liang, L. Yi, Z. Huang, B. Lu, C. Dan, R. Zhong, Effect of silica on reduction behaviors of hematite-carbon composite compact at 1223–1373 K, ISIJ Int 59 (2019) 227–234.
[10] H. Zhong, L. Wen, J. Li, J. Xu, M. Hu, Z. Yang, The adsorption behaviors of CO and H2 on FeO surface: a density functional theory study, Powder Technol. 303 (2016) 100–108.
[11] A. Alaoui Mouayd, A. Koltsov, E. Sutter, B. Tribollet, Effect of silicon content in steel and oxidation temperature on scale growth and morphology, Mater. Chem. Phys. 143 (2014) 996–1004.
[12] L. Suarez, J. Schneider, Y. Houbaert, High-temperature oxidation of Fe-Si alloys in the temperature range 900-1250 °C, DDF 273-276 (2008) 661–666.
[13] I.R. Souza Filho, H. Springer, Y. Ma, A. Mahajan, C.C. da Silva, M. Kulse, D. Raabe, Green steel at its crossroads: hybrid hydrogen-based reduction of iron ores, J. Clean. Prod. 340 (2022), 130805.
[14] A.A. El-Geassy, M.I. Nasr, E.A. Mousa, Influence of manganese oxide and silica on the morphological structure of hematite compacts, Steel Res. Int. 81 (2010) 178–185.
[15] M. Lattemann, U. Helmersson, J.E. Greene, Fully dense, non-faceted 111-textured high power impulse magnetron sputtering TiN films grown in the absence of substrate heating and bias, Thin Solid Films 518 (2010) 5978–5980.
[16] P. Ström, D. Primetzhofer, Ion beam tools for nondestructive in-situ and in-operando composition analysis and modification of materials at the Tandem Laboratory in Uppsala, J. Inst. 17 (2022) P04011.
[17] M.V. Moro, R. Holeňák, L. Zendejas Medina, U. Jansson, D. Primetzhofer, Accurate high-resolution depth profiling of magnetron sputtered transition metal alloy films containing light species: a multi-method approach, Thin Solid Films 686 (2019), 137416.
[18] M. Hans, H. Rueß, Z. Czigány, J. Krause, P. Ondračka, D. Music, S. Evertz, D. M. Holzapfel, D. Primetzhofer, J.M. Schneider, Spinodal decomposition of reactively sputtered (V0.64Al0.36)0.49N0.51 thin films, Surf. Coat. Technol. 389 (2020), 125641.
[19] D.A. Shirley, High-resolution X-Ray photoemission spectrum of the valence bands of gold, Phys. Rev. B 5 (1972) 4709–4714.
[20] Kratos Analytical Ltd., Relative sensitivity factors (RSF) for Kratos AXIS Supra.
[21] M.C. Biesinger, B.P. Payne, A.P. Grosvenor, L.W.M. Lau, A.R. Gerson, R.S.C. Smart, Resolving surface chemical states in XPS analysis of first row transition metals, oxides and hydroxides: Cr, Mn, Fe, Co and Ni, Appl. Surf. Sci. 257 (2011) 2717–2730.
[22] T. Yamashita, P. Hayes, Analysis of XPS spectra of Fe2+ and Fe3+ ions in oxide materials, Appl. Surf. Sci. 254 (2008) 2441–2449.
[23] G. Greczynski, L. Hultman, A step-by-step guide to perform x-ray photoelectron spectroscopy, J. Appl. Phys. 132 (2022) 11101.
[24] A. Saksena, S. Prünte, D.M. Holzapfel, L. Patterer, J.M. Schneider, Influence of glass contact induced changes in surface composition of Pt, PtIr and Ir protective coatings on glass adhesion, Appl. Surf. Sci. 548 (2021), 149282.
[25] J.E. Greene, J.-.E. Sundgren, L. Hultman, I. Petrov, D.B. Bergstrom, Development of preferred orientation in polycrystalline TiN layers grown by ultrahigh vacuum reactive magnetron sputtering, Appl. Phys. Lett. 67 (1995) 2928–2930.
[26] E. Wolska, U. Schwertmann, Nonstoichiometric structures during dehydroxylation of goethite, Z. Kristallogr. Cryst. Mater. 189 (1989) 223–237.
[27] M. Lübbe, A.M. Gigler, R.W. Stark, W. Moritz, Identification of iron oxide phases in thin films grown on Al2O3(0001) by Raman spectroscopy and X-ray diffraction, Surf. Sci. 604 (2010) 679–685.
[28] A. Anders, A structure zone diagram including plasma-based deposition and ion etching, Thin Solid Films 518 (2010) 4087–4090.
[29] A.W. Hull, A new method of X-ray crystal analysis, Phys. Rev. 10 (1917) 661–696.
[30] H. Fjellvåg, F. Grønvold, S. Stølen, B. Hauback, On the Crystallographic and magnetic structures of nearly stoichiometric iron monoxide, J. Solid State Chem. 124 (1996) 52–57.
[31] L.W. Finger, R.M. Hazen, A.M. Hofmeister, High-Pressure crystal chemistry of spinel (MgAl2O4) and magnetite (Fe3O4): comparisons with silicate spinels, Phys. Chem. Miner. 13 (1986) 215–220.